

# Refined stellar, orbital and planetary parameters of the eccentric HAT-P-2 planetary system

András Pál<sup>1,2,3\*</sup>, Gáspár Á. Bakos<sup>1†</sup>, Guillermo Torres<sup>1</sup>, Robert W. Noyes<sup>1</sup>, Debra A. Fischer<sup>4</sup>, John A. Johnson<sup>5</sup>, Gregory W. Henry<sup>6</sup>, R. Paul Butler<sup>7</sup>, Geoffrey W. Marcy<sup>8</sup>, Andrew W. Howard<sup>8</sup>, Brigitta Sipőcz<sup>1,3</sup>, David W. Latham<sup>1</sup> and Gilbert A. Esquerdo<sup>1</sup>

<sup>1</sup> *Harvard-Smithsonian Center for Astrophysics, 60 Garden street, Cambridge, MA, 02138, USA*

<sup>2</sup> *Konkoly Observatory of the Hungarian Academy of Sciences, Konkoly Thege Miklós út 15-17, Budapest, 1121, Hungary*

<sup>3</sup> *Department of Astronomy, Loránd Eötvös University, Pázmány P. st. 1/A, Budapest, 1117, Hungary*

<sup>4</sup> *Department of Physics and Astronomy, San Francisco State University, San Francisco, CA, 94132, USA*

<sup>5</sup> *Institute for Astronomy, University of Hawaii, Honolulu, HI, 96822, USA*

<sup>6</sup> *Center of Excellence in Information Systems, Tennessee State University, Nashville, TN 37209, USA*

<sup>7</sup> *Department of Terrestrial Magnetism, Carnegie Institute of Washington, Washington DC, 20015, USA*

<sup>8</sup> *Department of Astronomy, University of California, Berkeley, CA, 94720, USA*

Accepted ..., received ...; in original form ...

## ABSTRACT

We present refined parameters for the HAT-P-2(b) extrasolar planetary system (also known as HD 147506(b)), based on new radial velocity and photometric data. HAT-P-2b is a transiting extrasolar planet (TEP) that exhibits an eccentric orbit. We present detailed analysis of the planetary and stellar parameters, yielding consistent results of the mass and radius of the star, better constraints on the orbital eccentricity and refined planetary parameters. Namely, the refined stellar parameters are  $M_{\star} = 1.36 \pm 0.04 M_{\odot}$  and  $R_{\star} = 1.64^{+0.09}_{-0.08} R_{\odot}$ , while the planet has a mass of  $M_p = 9.09 \pm 0.24 M_{\text{Jup}}$  and radius of  $R_p = 1.157^{+0.073}_{-0.092} R_{\text{Jup}}$ . The refined ephemeris for the planet are  $E = 2,454,387.49375 \pm 0.00074$  (BJD) and  $P = 5.6334729 \pm 0.0000061$  (days) while the newly obtained orbital eccentricity and argument of pericenter are  $e = 0.5171 \pm 0.0033$  and  $\omega = 185.22^{\circ} \pm 0.95^{\circ}$ . These orbital elements allow us to predict the timings of secondary eclipses with a reasonable accuracy. We also discuss effects of this significant eccentricity, such as the time-lag between the radial velocity and photometry based transit centers, or the asymmetry in the transit light curve. Simple formulae are presented for the above, and these, in turn, can be used to constrain the orbital eccentricity using purely photometric data. These will be particularly useful for very high precision, space-borne observations of TEPs.

**Key words:** planetary systems — stars: fundamental parameters — stars: individual: HD 147506, HAT-P-2 – techniques: spectroscopic

## 1 INTRODUCTION

At the time of its discovery, HAT-P-2b was the longest period and most massive transiting extrasolar planet (TEP), and the only one known to exhibit an eccentric orbit (Bakos et al. 2007a). In the following years, other TEPs have also been discovered with significant orbital eccentricity,

and long period: GJ 436b (Gillon et al. 2007), HD 17156b (Barbieri et al. 2007), XO-3b (Johns-Krull et al. 2008) and HD 80606 (Naef et al. 2001; Winn et al. 2009b). See, e.g. <http://exoplanet.eu> for an up-to-date database for transiting extrasolar planets.

The planetary companion to HAT-P-2 (also HD 147506) was detected as a transiting object during the campaign of the HATNet telescopes (Bakos et al. 2002, 2004), and Wise HAT telescope (WHAT Shporer et al. 2006). The HATNet telescopes located at Fred Lawrence Whipple Observatory

\* E-mail: apal@szofi.net

† NSF fellow

(FLWO), and Mauna Kea and the WHAT telescope gathered  $\sim 26,000$  individual photometric measurements with good signal-to-noise ratio (SNR). The planetary transit was followed up by the FLWO 1.2m telescope, utilizing the KeplerCam detector. The planetary properties have been confirmed by radial velocity measurements and bisector analysis of the spectral line profiles. The latter has shown no bisector variations, excluding the possibilities of blended scenarios of three or more stars, such as a hierarchical triple.

Recently, the spin-orbit alignment of the HAT-P-2(b) system was measured by Winn et al. (2007a) and Loeillet et al. (2008). Both studies reported an alignment consistent with zero within an uncertainty of  $\sim 10^\circ$ . These results are exceptionally interesting since short period planets are thought to be formed at much larger distances from their parent star and migrated inward, while the orbital eccentricity is damped yielding an almost circular orbit (D’Angelo, Lubow & Bate 2006). Physical mechanisms such as Kozai interaction between the transiting planet and an unknown massive companion on an inclined orbit could result tight eccentric orbits (Fabrycky & Tremaine 2007; Takeda, Kita & Rasio 2008). However, in such a scenario, the spin-orbit alignment can be expected to be significantly larger than the measured. For instance, in the case of XO-3b, the reported alignments are  $\lambda = 70^\circ \pm 15^\circ$  (Hébrard et al. 2008) and  $\lambda = 37.3^\circ \pm 3.7^\circ$  (Winn et al. 2009a, however, there are indications for systematic observational effects). In multiple planetary systems, planet-planet scattering can also yield eccentric orbits (see e.g. Ford & Rasio 2008).

The physical properties of the host star HAT-P-2 have been controversial, since different methods for stellar characterization resulted stellar radii between  $\sim 1.4 R_\odot$  and  $\sim 1.8 R_\odot$ . Moreover, the actual distance of the system also had large systematic errors, since the reported Hipparcos distance seemed to be significantly larger than what could be expected from the absolute luminosity (coming from the stellar evolution modeling).

In this paper we present new photometric and spectroscopic observations of the planetary system HAT-P-2(b). The new photometric measurements significantly improve the light curve parameters, therefore some of the stellar parameters are more accurately constrained. In addition, radial velocity measurements based on spectroscopic observations have resulted significantly smaller uncertainties, which, due to the orbital eccentricity, also affect the results of the stellar evolution modeling. In § 2, we summarize our photometric observations of this system, while in § 3 we briefly describe the issues related to the radial velocity data points. The details of the analysis are discussed in § 4. We summarize our results in § 5.

## 2 PHOTOMETRIC OBSERVATIONS AND REDUCTIONS

In the present analysis we utilize photometric data obtained by the HATNet telescopes, by the KeplerCam detector mounted on the FLWO 1.2m telescope, by the Nickel 1 m telescope at Lick Observatory on Mount Hamilton, California and by four of the automated photometric telescopes (APTs) at Fairborn Observatory in southern Arizona. The photometry of HATNet have already been presented in

Bakos et al. (2007a). These HATNet data are plotted on Fig. 1, superimposed with our new best-fit model (see § 4 for details on light curve modeling). We observed the planetary transit nine times, on 2007 March 18<sup>1</sup> (Sloan’s  $z$  band), 2007 April 21 ( $z$ ), 2007 May 08 ( $z$ ), 2007 June 22 ( $z$ ), 2008 March 24 ( $z$ ), 2008 May 25 ( $z$ ), 2008 July 26 ( $z$ ), 2009 April 28 (Strömgren  $b + y$  band) and 2009 May 15 ( $b + y$ ), yielding 6 complete or nearly complete and 3 partial transit light curves. One of these follow-up light curves (2007 April 21) has already been published in the discovery paper. All of our individual high precision follow-up photometry data are plotted on Fig. 2, along with our best-fit transit light curve model (see also § 4), while the folded and binned light curve (computed only for the  $z$ -band observations) is displayed on Fig. 3.

The frames taken by the KeplerCam detector have been calibrated and reduced in the same way all for the six nights at FLWO, described as follows. Prior to the real calibration, all pixels which are saturated (or “bloomed”) have been marked, forcing them to be omitted from the upcoming photometry. During the calibration of the frames we used the standard bias, dark and sky-flat corrections.

Following the calibration, the detection of stars and the derivation of the astrometrical solution was done in two steps. First, an initial astrometrical transformation was derived using the  $\sim 50$  brightest and non-saturated stars from each frame, and by using the 2MASS catalogue (Skrutskie 2006) as a reference. We utilized the algorithm of Pál & Bakos (2006) with a second-order polynomial fit. Since the astrometrical data found in the 2MASS catalogue was obtained by the same kind of telescope in diameter (thus, the expectations for the signal-to-noise is roughly the same), one could expect significantly better astrometrical data from the FLWO 1.2 m due to the numerous individual frames taken. Indeed, an internal catalog which was derived from the detected stellar centroids by registering them to the same reference system has shown an internal precision  $\sim 0.005$  arc sec for the brighter stars, while the 2MASS catalog reports an uncertainty larger by an order of magnitude: nearly  $\sim 0.06$  arc sec. Therefore, in the second step of the astrometry, we used this new catalog to derive the individual astrometrical solutions for each frame, still using a second-order polynomial fit. We note here that this method also corrects for the systematic errors in the photometry yielded by the proper motion of the stars that has changed their position since the epoch of the 2MASS catalogue ( $\sim 2000$ ).

Using the astrometrical solutions above we performed aperture photometry on fix centroids, employing a set of five apertures between 7.5 and 17.5 pixels in radius. The results of the aperture photometry were then transformed to the same instrumental magnitude system using a correction to the spatial distortions and the differential extinction (the former depends on the celestial coordinates while the latter depends on the intrinsic colors of the stars). Both corrections were linear in the pixel coordinates and linear in the colors. Experience shows that significant correlations can occur between the instrumental magnitudes and some of the external parameters of the light curves (such as the FWHM

<sup>1</sup> All of the dates are local (MST or HT) calendar dates for the first half of the night.

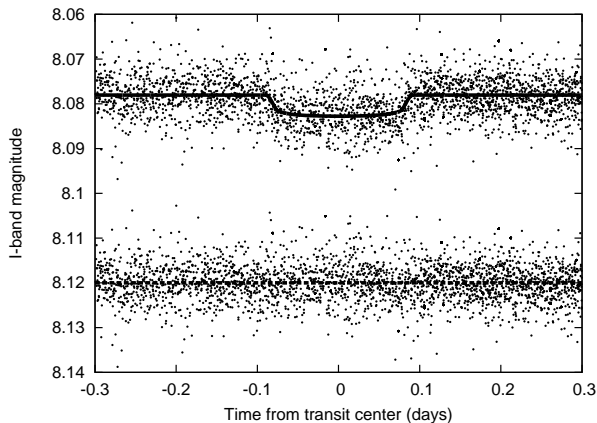


**Figure 1.** The folded HATNet light curve of HAT-P-2 (published in Bakos et al. 2007a), showing the points only nearby the transit. The upper panel is superimposed with our best-fit model and the lower panel shows the fit residual. See text for further details.

of the stars, subpixel positions). Although one should detrend against these correlations using purely out-of-transit data (both before ingress and after egress), we have carried out such an external parameter decorrelation (EPD) simultaneously with the light curve modeling (§ 4) due to the lack of out-of-transit data in several cases (see Bakos et al. 2009). After the simultaneous light curve modelling and detrending, we chose the aperture for each night that yielded the smallest residual. In all of the cases this “best aperture” was neither the smallest nor the largest one from the set, confirming our assumptions for selecting a good aperture series. We note here that since all of the stars on the frames were well isolated, such choice of different radii of the apertures does not induce systematics related to variable blending of stars in different apertures. In addition, due to the high apparent brightness of HAT-P-2 and the comparison stars, the frames were acquired under a slightly extrafocal setting (in order to avoid saturation). This resulted in a different characteristic FWHM for each night, thus the optimal apertures yielding the highest signal-to-noise ratio also have different radii for each night. Additional and more technical details about the complete photometric process utilized in this particular and related data reductions are discussed in Chapter 2 of Pál (2009b).

For the observation at Lick Observatory, we used the Nickel Direct Imaging Camera, which is a thinned Loral 2048<sup>2</sup> CCD with a 6.3′ square field of view. We observed through a Gunn Z filter, and used 2 × 2 binning for an effective pixel scale of 0′.37 pixel<sup>−1</sup>. The exposure times were 25 s, with a readout and refresh time between exposures of 12 s. The conditions were clear for most of this transit with ∼ 1′.0 seeing. We defocused the images to draw out the exposure time while avoiding saturation for the target and reference stars. We applied the flat-field and bias calibrations, and determined the instrumental magnitude of HAT-P-2 using custom routines written in IDL as described previously by Winn et al. (2007b) and Johnson et al. (2008). We measured the flux of the target relative to two comparison stars using an aperture with an 17 pixel radius and a sky background annulus extending from 18 to 60 pixels.

All four of the APTs at Fairborn Observatory have two channel photometers that measure the Strömgren *b* and Strömgren *y* count rates simultaneously (Henry 1999). Since the Strömgren *b* and *y* bands are fairly close together and don’t provide any useful color information for such shallow transits, we averaged the *b* and *y* differential magnitudes to create a  $(b + y)/2$  “band pass” and that gives roughly a  $\sqrt{2}$  improvement in precision. The comparison star for all of the APT observations is HD 145435.

### 3 RADIAL VELOCITY OBSERVATIONS

In the discovery paper of HAT-P-2b (Bakos et al. 2007a), 13 individual radial velocity measurements were reported that were utilizing the HIRES instrument (Vogt et al. 1994) on the Keck I telescope, on Mauna Kea, Hawaii, plus 10 measurements from the Hamilton echelle spectrograph at the Lick Observatory (Vogt 1987). In the last year, we have acquired 14 additional radial velocity measurements using the HIRES instrument on Keck. In the analysis, we have also used the on-line radial velocity data obtained by the OHP/SOPHIE spectrograph at out-of-transit (i.e. omitting the measurements for the Rossiter-McLaughlin effect), published by Loeillet et al. (2008). With these additional 8 observations, we have 27 + 10 + 8 = 45 high precision RV data points at hand for a refined analysis.

In Table 1 we collected all (previously published and our newly obtained) radial velocity measurements. On Fig. 4 we show the RV data, over-plotted with our best-fit model solution (for details of the fit, see § 4).

### 4 ANALYSIS

In this section we describe the analysis of the available photometric and radial velocity data in order to determine the planetary parameters as accurately as possible. The modeling was done in three steps. The first step was the modeling of the light curve and the radial velocity data series. Second, this was followed by the determination of the stellar parameters. In the last step, by combining the light curve parameters with the stellar properties, we obtained the physical parameters (mass, radius) of the planet.

To model transit light curves taken in optical or near-infrared photometric passbands, we include the effect of the stellar limb darkening. We have used the analytic formulae of Mandel & Agol (2002) to model the flux decrease during transits under the assumption of quadratic limb darkening law. Since the limb darkening coefficients are the function of the stellar atmospheric parameters (such as effective temperature  $T_{\text{eff}}$ , surface gravity  $\log g_*$  and metallicity), the whole light curve analysis is preceded by the initial derivation of these parameters using the iodine-free template spectrum obtained by the HIRES instrument on Keck I. We employed the Spectroscopy Made Easy software package (SME, see Valenti & Piskunov 1996), supported by the atomic line database of Valenti & Fischer (2005). This analysis yields the  $T_{\text{eff}}$ ,  $\log g_*$ , [Fe/H] and the projected rotational velocity  $v \sin i$ . The initial result of the SME analysis when all of these values have been adjusted simultaneously were  $\log g_* = 4.22 \pm 0.14$  (CGS),  $T_{\text{eff}} = 6290 \pm 110$  K,

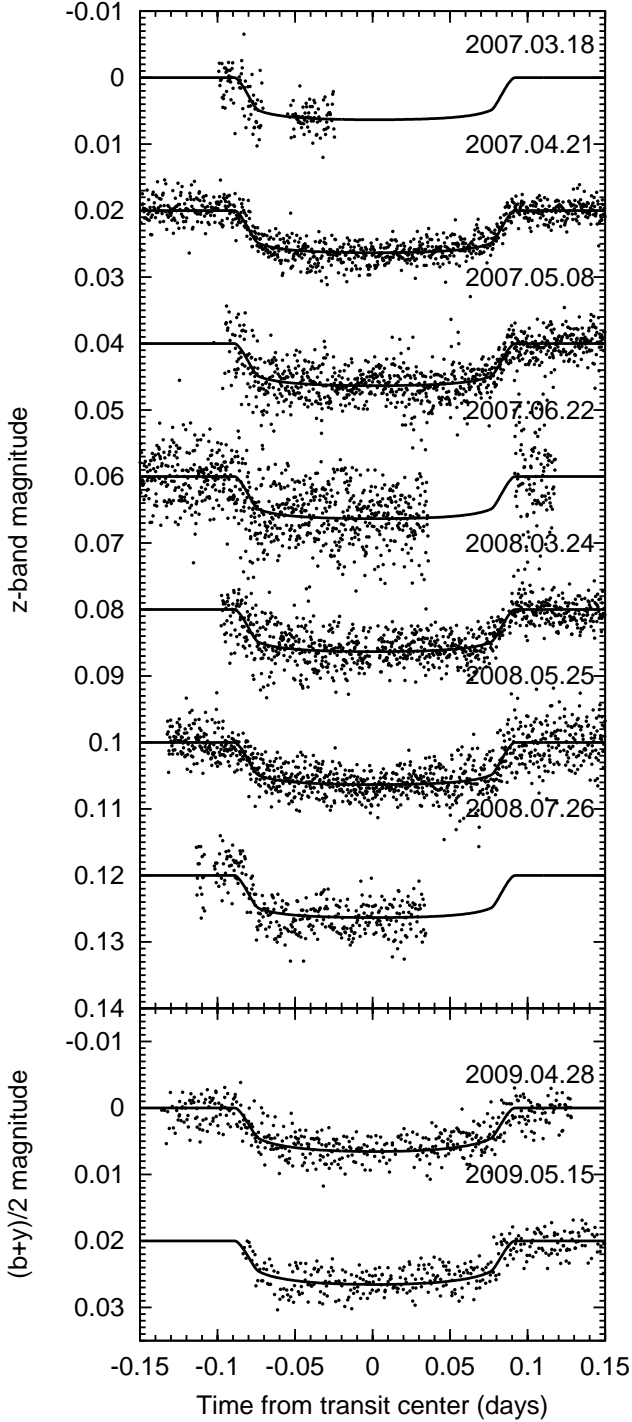


**Figure 2.** Follow-up light curves of HAT-P-2. The top panel shows the  $z$  band light curves acquired on 2007 March 18, 2007 April 21, 2007 May 08, 2007 June 22, 2008 March 24, 2008 May 25 and 2008 July 26, while the respective transit sequence numbers were  $N_{\text{tr}} = -6, 0, +3, +11, +60, +71$  and  $+82$ . The lower panel shows the Strömgren  $(b+y)/2$  light curves, acquired on 2009 April 28 and 2009 May 15, while the respective transit sequence numbers were  $N_{\text{tr}} = +131$  and  $+134$ . All of these light curves are superimposed with our best-fit model. See text for further details.

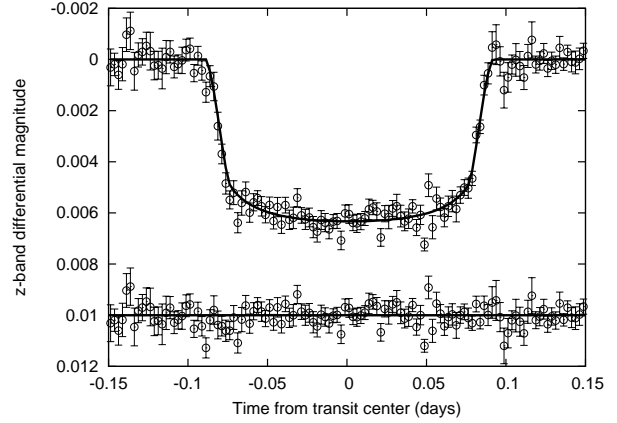


**Figure 3.** Folded and binned follow-up light curve of HAT-P-2, calculated from the seven individual  $z$ -band measurements. The flux values at each point have been derived from  $\sim 35 - 50$  individual measurements and the bin size is equivalent with a cadence of 3.6 minutes (that is, 0.0025 days). The errorbars are derived from the statistical scatters from the points happens to fall in the given bin. The overall magnitude of these uncertainties are  $\sim 0.4$  mmag.

$[\text{Fe}/\text{H}] = 0.12 \pm 0.08$  and  $v \sin i = 20.8 \pm 0.2 \text{ km s}^{-1}$ . The limb darkening coefficients were then derived for  $z'$ ,  $I$  and  $(b+y)/2$  photometric bands by interpolation, using the tables provided by Claret (2000) and Claret (2004). The initial values for the coefficients were used in the subsequent global modeling of the data (§ 4.1), and also in refining the stellar parameters through a constraint on the mean stellar density (see later). A second SME iteration was then performed with fixed stellar surface gravity. The final limb darkening parameters are:  $\gamma_1^{(z)} = 0.1419$ ,  $\gamma_2^{(z)} = 0.3634$ ,  $\gamma_1^{(b+y)} = 0.4734$ ,  $\gamma_2^{(b+y)} = 0.2928$ ,  $\gamma_1^{(I)} = 0.1752$ , and  $\gamma_2^{(I)} = 0.3707$ .

#### 4.1 Light curve and radial velocity parameters

The first step of the analysis is the determination of the light curve and radial velocity parameters. The parameters can be classified into three groups. The light curve parameters that are related to the *physical* properties of the planetary system are the transit epoch  $E$ , the period  $P$ , the fractional planetary radius  $p \equiv R_p/R_*$ , the impact parameter  $b$ , and the normalized semi-major axis  $a/R_*$ . The physical radial velocity parameters are the RV semi-amplitude  $K$ , the orbital eccentricity  $e$  and the argument of pericenter  $\omega$ . In the third group there are parameters that are not related to the physical properties of the system, but are rather instrumentation specific ones. These are the out-of-transit instrumental magnitudes of the followup (and HATNet) light curves, and the RV zero-points  $\gamma_{\text{Keck}}$ ,  $\gamma_{\text{Lick}}$  and  $\gamma_{\text{OHP}}$  of the three individual data sets<sup>2</sup>.

<sup>2</sup> Since in the reduction of the Loeillet et al. (2008) data a synthetic stellar spectrum were used as a reference,  $\gamma_{\text{OHP}}$  is the physical barycentric radial velocity of the system. In the reductions of the Keck and Lick data, we used one of the spectra as a template, therefore the zero-points of these two are arbitrary, and lack any real physical interpretation.

**Table 1.** Comprehensive list of relative radial velocity measurements for HAT-P-2

BJD	RV m s <sup>-1</sup>	$\sigma_{RV}$ m s <sup>-1</sup>	Observatory
2453981.77748	12.0	7.3	Keck <sup>a</sup>
2453982.87168	-288.3	7.9	Keck <sup>a</sup>
2453983.81485	569.0	7.3	Keck <sup>a</sup>
2454023.69150	727.3	7.8	Keck <sup>a</sup>
2454186.99824	721.3	7.7	Keck <sup>a</sup>
2454187.10415	711.0	6.7	Keck <sup>a</sup>
2454187.15987	738.1	6.8	Keck <sup>a</sup>
2454188.01687	783.6	7.1	Keck <sup>a</sup>
2454188.15961	801.8	6.7	Keck <sup>a</sup>
2454189.01037	671.0	6.7	Keck <sup>a</sup>
2454189.08890	656.7	6.8	Keck <sup>a</sup>
2454189.15771	640.2	6.9	Keck <sup>a</sup>
2454216.95938	747.7	8.1	Keck
2454279.87688	402.0	8.3	Keck
2454285.82384	168.3	5.7	Keck
2454294.87869	756.8	6.5	Keck
2454304.86497	615.5	6.2	Keck
2454305.87010	764.2	6.3	Keck
2454306.86520	761.4	7.6	Keck
2454307.91236	479.1	6.5	Keck
2454335.81260	574.7	6.8	Keck
2454546.09817	-670.9	10.1	Keck
2454547.11569	554.6	7.4	Keck
2454549.05046	784.8	9.2	Keck
2454602.91654	296.3	7.0	Keck
2454603.93210	688.0	5.9	Keck
2454168.96790	-152.7	42.1	Lick <sup>a</sup>
2454169.95190	542.4	41.3	Lick <sup>a</sup>
2454170.86190	556.8	42.6	Lick <sup>a</sup>
2454171.03650	719.1	49.6	Lick <sup>a</sup>
2454218.80810	-1165.2	88.3	Lick <sup>a</sup>
2454218.98560	-1492.6	90.8	Lick <sup>a</sup>
2454219.93730	-28.2	43.9	Lick <sup>a</sup>
2454219.96000	-14.8	43.9	Lick <sup>a</sup>
2454220.96410	451.6	38.4	Lick <sup>a</sup>
2454220.99340	590.7	37.1	Lick <sup>a</sup>
2454227.50160	-19401.4	8.8	OHP <sup>b</sup>
2454227.60000	-19408.2	6.5	OHP <sup>b</sup>
2454228.58420	-19558.1	18.8	OHP <sup>b</sup>
2454229.59930	-20187.4	16.1	OHP <sup>b</sup>
2454230.44750	-21224.9	14.1	OHP <sup>b</sup>
2454230.60290	-20853.6	14.8	OHP <sup>b</sup>
2454231.59870	-19531.1	12.1	OHP <sup>b</sup>
2454236.51900	-20220.7	5.6	OHP <sup>b</sup>

<sup>a</sup> Published in Bakos et al. (2007a).<sup>b</sup> Published in Loeillet et al. (2008).

To minimize the correlation between the adjusted parameters, we use a slightly different parameter set. Instead of adjusting the epoch and period, we fitted the first and last available transit center time,  $T_{-148}$  and  $T_{+134}$ . Here indices note the transit event number: the  $N_{tr} \equiv 0$  event was defined as the first complete follow-up light curve taken on 2007 April 21, the first available transit observation from the HATNet data was the event  $N_{tr} \equiv -148$  and the last complete follow-up was observed on 2009 May 15, was event  $N_{tr} \equiv +134$ . Note that assuming equidistant transit events, all of the transit centers available in the HATNet and follow-

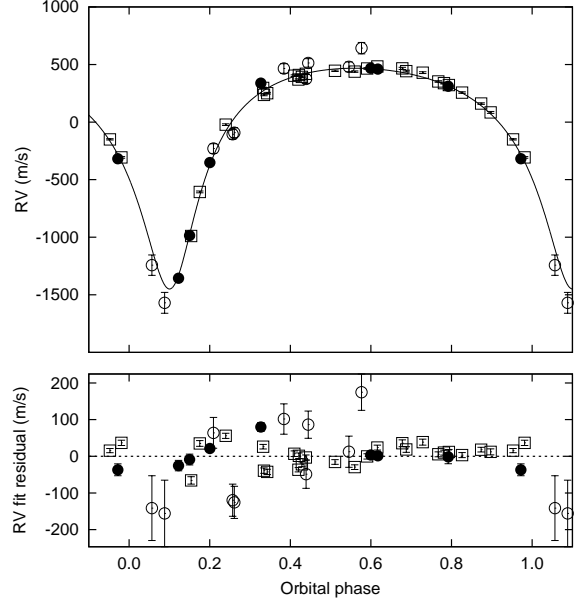


**Figure 4.** Radial velocity measurements for HAT-P-2 folded with the best-fit orbital period. Filled dots represent the OHP data, open circles show the the Lick/Hamilton, while the open boxes mark the Keck/HIRES observations. In the upper panel, all of these three RV data sets are shifted to zero mean barycentric velocity. The RV data are superimposed with our best-fit model. The lower panel shows the residuals from the best-fit. Note the different vertical scales on the two panels. The transit occurs at zero orbital phase. See text for further details.

up photometry are constrained by these two transit instances (see Bakos et al. 2007b; Pál et al. 2008a). Similarly, instead of the eccentricity  $e$  and argument of pericenter  $\omega$ , we have adjusted the Lagrangian orbital elements  $k \equiv e \cos \omega$  and  $h \equiv e \sin \omega$ . These elements show no correlation in practice, moreover, the radial velocity curve is an analytic function of these even for  $e \rightarrow 0$  cases (Pál 2009a). As it is known in the literature (Winn et al. 2007b; Pál 2008), the impact parameter  $b$  and  $a/R_*$  are also strongly correlated, especially for small  $p \equiv R_p/R_*$  values. Therefore, as it was suggested by Bakos et al. (2007b), we chose the parameters  $\zeta/R_*$  and  $b^2$  for fitting instead of  $a/R_*$  and  $b$ , where for eccentric orbits  $\zeta/R_*$  is related to  $a/R_*$  as

$$\frac{\zeta}{R_*} = \left( \frac{a}{R_*} \right) \frac{2\pi}{P} \frac{1}{\sqrt{1-b^2}} \frac{\sqrt{1-e^2}}{1+h}. \quad (1)$$

The quantity  $\zeta/R_*$  is related to the transit duration as  $T_{dur} = 2(\zeta/R_*)^{-1}$ , if the duration is defined between the time instants when the center of the planet crosses the limb of the star inwards and outwards, respectively.

The actual flux decrease caused by the transiting planet can be estimated from the projected radial distance between the center of the planet and the center of the star  $d$  (normalized by  $R_*$ ). For circular orbits the time dependence of  $d$  is trivial (see e.g. Mandel & Agol 2002). For eccentric orbits, it is necessary to use precise parametrization of  $d$  as a function of time. As it was shown in Pál (2008),  $d$  can be parametrized in a second order approximation as

$$d^2 = (1 - b^2) \left( \frac{\zeta}{R_\star} \right)^2 (\Delta t)^2 + b^2, \quad (2)$$

where  $\Delta t$  is the time between the actual observation time and the RV-based transit center. Here the *RV-based transit center* is defined when the planet reaches its maximal tangential velocity during the transit. Throughout this paper, we give the ephemeris for the RV-based transit centers and denote these simply by  $T_c$ . Although the tangential velocity cannot be measured directly, the RV-based transit center is constrained purely by the radial velocity data, without any knowledge of the transit geometry<sup>3</sup>. For eccentric orbits the impact parameter  $b$  is related to the orbital inclination  $i$  as

$$b = \left( \frac{a}{R_\star} \right) \cos i \frac{1 - e^2}{1 + h}. \quad (3)$$

In order to have a better description of the transit light curve, we used a higher order expansion in the  $d(\Delta t)$  function (Eq. 2). For circular orbits, such an expansion is straightforward. To derive the expansion for elliptic orbits, we employed the method of Lie-integration which gives the solution of any ordinary differential equation (here, the equations for the two-body problem) in a recursive series for the Taylor expansion with respect to the independent variable (here, the time). By substituting the initial conditions for a body of which spatial coordinates are written as the functions of the orbital elements, using equations (C1)-(C8) of Pál & Süli (2007), one can derive that the normalized projected distance  $d$  up to fourth order is:

$$d^2 = b^2 \left[ 1 - 2R\varphi - (Q - R^2)\varphi^2 - \frac{1}{3}QR\varphi^3 \right] + \left( \frac{\zeta}{R_\star} \right)^2 (1 - b^2) \Delta t^2 \left[ 1 - \frac{1}{3}Q\varphi^2 + \frac{1}{2}QR\varphi^3 \right], \quad (4)$$

where

$$Q = \left( \frac{1 + h}{1 - e^2} \right)^3, \quad (5)$$

and

$$R = \frac{1 + h}{(1 - e^2)^{3/2}} k. \quad (6)$$

Here  $n = 2\pi/P$  is the mean motion, and  $\varphi$  is defined as  $\varphi = n\Delta t$ . For circular orbits,  $Q = 1$  and  $R = 0$ , and for small eccentricities ( $e \ll 1$ ),  $Q \approx 1 + 3h$  and  $R \approx k$ .

## 4.2 Joint fit

Given the physical model parametrized above, we performed a simultaneous fit on all of the light curve and radial velocity data. We have involved Eq. (4), to model the light curves, where the parameters  $Q$  and  $R$  were derived from the actual values of  $k$  and  $h$ , using equations Eq. (5) and Eq. (6). To find the best-fit values for the parameters we used the downhill simplex algorithm (see Press et al. 1992) and we used the method of refitting to synthetic data sets to get an *a posteriori* distribution for the adjusted values.

<sup>3</sup> In other words, predictions can only be made for the RV-based transit center in the cases where the planet was discovered by a radial velocity survey and initially there are no further constraints for the geometry of the system, notably its impact parameter

The final results of the fit were  $T_{-148} = 2453379.10210 \pm 0.00121$ ,  $T_{+134} = 2454967.74146 \pm 0.00093$ ,  $K = 983.9 \pm 17.2 \text{ m s}^{-1}$ ,  $k = -0.5152 \pm 0.0036$ ,  $h = -0.0441 \pm 0.0084$ ,  $R_p/R_\star \equiv p = 0.07227 \pm 0.00061$ ,  $b^2 = 0.156 \pm 0.074$ ,  $\zeta/R_\star = 12.147 \pm 0.046 \text{ day}^{-1}$ ,  $\gamma_{\text{Keck}} = 316.0 \pm 6.0 \text{ m s}^{-1}$ ,  $\gamma_{\text{Lick}} = 88.9 \pm 10.4 \text{ m s}^{-1}$ ,  $\gamma_{\text{OHP}} = -19860.5 \pm 10.2 \text{ m s}^{-1}$ . The uncertainties of the out-of-transit magnitudes were between  $(6 \dots 21) \times 10^{-5} \text{ mag}$  for the follow-up light curves and  $16 \times 10^{-5} \text{ mag}$  for the HATNet data. The fit resulted a normalized  $\chi^2$  value of 0.992. As it is described in the following subsection, the resulted distribution has been used then as an input for the stellar evolution modeling.

## 4.3 Effects of the orbital eccentricity on the transit

In this section we summarize how the orbital eccentricity affects the shape of the transit light curve. The presented analysis is related to the quantification of this distortion in the photometric data. The leading order correction term in Eq. (4) in  $\varphi$ ,  $-2b^2 R\varphi$ , is related to the time lag between the *photometric* and RV-based transit centers (see also Kopal 1959). The photometric transit center, denoted as  $T_{c,\text{phot}}$  is defined halfway between the instants when the center of the planet crosses the limb of the star inward and outward. It is easy to show by solving the equation  $d(\varphi) = 1$ , yielding two solutions ( $\varphi_I$  and  $\varphi_E$ ), that this phase lag is:

$$\Delta\varphi = \frac{\varphi_I + \varphi_E}{2} = \quad (7)$$

$$= -\frac{b^2 R}{\left( \frac{\zeta}{R_\star} \frac{1}{n} \right)^2 (1 - b^2) - (Q - R^2)b^2} \approx \quad (8)$$

$$\approx -\left( \frac{a}{R_\star} \right)^{-2} \frac{b^2 k}{(1 + h)\sqrt{1 - e^2}}, \quad (9)$$

which can result in a time lag of several minutes. For instance, in the case of HAT-P-2b,  $T_{c,\text{phot}} - T_{c,\text{RV}} = n^{-1} \Delta\varphi = 1.6 \pm 0.9 \text{ minutes}$ .

In Eq. (4), the third order terms in  $\varphi$  describe the asymmetry between the slopes of the ingress and egress parts of the light curve. For some other aspects of light curve asymmetries see Loeb (2005) and Barnes (2007). In the cases when no assumptions are known for the orbital eccentricity (such as no RV data available), we cannot treat the parameters  $R$  and  $Q$  as independent since the photometric transit center and  $R$  have an exceptionally high correlation. However, if we assume a simpler model function, with only third order terms in  $\varphi$  with fitted coefficients present, i.e.

$$d^2 = b^2 \left[ 1 - \varphi^2 - \frac{1}{3}C\varphi^3 \right] + \left( \frac{\zeta}{R_\star} \right)^2 (1 - b^2) \Delta t^2 \left[ 1 - \frac{1}{3}\varphi^2 + \frac{1}{2}C\varphi^3 \right], \quad (10)$$

these will yield a non-zero value for the  $C$  coefficient for asymmetric light curves. In the case of HAT-P-2b, the derived values for  $Q$  and  $R$  are  $Q = 2.204 \pm 0.074$  and  $R = -0.784 \pm 0.015$  (derived from the values of  $k$  and  $h$ , see § 4.2), thus the coefficient for the third order term in  $\varphi$  will be  $QR = -1.73 \pm 0.09$ . Using Eq. (10), for an “ideal” light curve (with similar parameters of  $k$ ,  $h$ ,  $\zeta/R_\star$  and  $b^2$  as for HAT-P-2b), the best fit value for  $C$  will be  $C = -2.23$ ,

**Table 2.** Stellar parameters for HAT-P-2.

Parameter	Value	Source
$T_{\text{eff}}$ (K)	$6290 \pm 60$	SME <sup>a</sup>
[Fe/H]	$+0.14 \pm 0.08$	SME
$\log g_*$ (cgs)	$4.16 \pm 0.03$	SME
$v \sin i$ (km s <sup>-1</sup> )	$20.8 \pm 0.3$	SME
$M_*$ ( $M_\odot$ )	$1.36 \pm 0.04$	Y <sup>2</sup> +LC+SME <sup>b</sup>
$R_*$ ( $R_\odot$ )	$1.64^{+0.09}_{-0.08}$	Y <sup>2</sup> +LC+SME
$\log g_*$ (cgs)	$4.138 \pm 0.035$	Y <sup>2</sup> +LC+SME
$L_*$ ( $L_\odot$ )	$3.78^{+0.48}_{-0.38}$	Y <sup>2</sup> +LC+SME
$M_V$ (mag)	$3.31 \pm 0.13$	Y <sup>2</sup> +LC+SME
Age (Gyr)	$2.6 \pm 0.5$	Y <sup>2</sup> +LC+SME
Distance (pc)	$119 \pm 8$	Y <sup>2</sup> +LC+SME

<sup>a</sup> SME = “Spectroscopy Made Easy” package for analysis of high-resolution spectra by Valenti & Piskunov (1996). See text.

<sup>b</sup> Y<sup>2</sup>+LC+SME = Yale-Yonsei isochrones (Yi et al. 2001), light curve parameters, and SME results.

which is close to the value of  $QR \approx -1.73$ . The difference between the best fit value of  $C$  and the fiducial value of  $QR$  is because in Eq. (10) the coefficients for the first and second order terms were fixed to be 0 and 1, respectively.

Although this asymmetry can be measured directly (without leading to any degeneracy between the fit parameters), in practice we need extreme photometric precision to obtain a significant detection for a non-zero  $C$  parameter: assuming a photometric time series for a single transit of HAT-P-2b with 5 sec cadence where each individual measurement has a photometric error of 0.01 mmag(!), the uncertainty in  $C$  will be  $\pm 0.47$ , equivalent to a 5- $\sigma$  detection of the light curve asymmetry. This detection would be hard for ground-based instrumentation (i.e. for a 1- $\sigma$  detection one should achieve a photometric precision of 0.05 mmag at the same cadence). Space missions such as *Kepler* (Borucki et al. 2007) will be able to detect orbital eccentricity of other planets relying only on photometry of primary transits.

#### 4.4 Stellar parameters

The second step of the analysis was the derivation of the physical stellar parameters. As it was pointed out by Sozzetti et al. (2007), the ratio  $a/R_*$  is a more effective luminosity indicator than the stellar surface gravity: in the cases where the mass of the transiting planet is negligible, the stellar density is

$$\rho_* \approx \frac{3\pi}{GP^2} \left( \frac{a}{R_*} \right)^3. \quad (11)$$

The normalized semi-major axis  $a/R_*$  can be obtained from the transit light curve model parameters, the orbital eccentricity and the argument of pericenter, see e.g. Eq. (1).

Since HAT-P-2b is a quite massive planet, i.e.  $M_p/M_* \sim 0.01$ , relation (11) requires a significant correction, which also depends on observable quantities (see Pál et al. 2008b, for more details). In the case of HAT-P-2b, this correction is not negligible since  $M_p/M_*$  is comparable to the typical relative uncertainties in the light curve parameters. As it is presented by Pál et al. (2008a), the density of the star is

$$\rho_* = \rho_0 - \frac{\Sigma_0}{R_*}, \quad (12)$$

where both  $\rho_0$  and  $\Sigma_0$  are observables, namely

$$\rho_0 = \frac{3\pi}{GP^2} \left( \frac{a}{R_*} \right)^3, \quad (13)$$

$$\Sigma_0 = \frac{3K\sqrt{1-e^2}}{2PG \sin i} \left( \frac{a}{R_*} \right)^2. \quad (14)$$

In Eq. (12), the only unknown quantity is the radius of the star, which can be derived using a stellar evolution model, and it depends on a luminosity indicator (which, in practice is the surface gravity or the density of the star), effective surface temperature,  $T_{\text{eff}}$  (given by the SME analysis) and the stellar composition (here [Fe/H]). Therefore, one can write

$$R_* = R_*(\rho_*, T_{\text{eff}}, [\text{Fe/H}]). \quad (15)$$

Since both  $T_{\text{eff}}$  and [Fe/H] are known, Eq. (12) and Eq. (15) have two unknowns, this set of equations can be solved iteratively. Note that in order to solve Eq. (15), supposing its parameters are known in advance, one has to use a certain stellar evolutionary model. Such models are available in tabulated form, therefore the solution of the equation requires the inversion of the interpolating function on the tabulated data. Thus, Eq. (15) is only a symbolical notation for the algorithm which provides the solution. Moreover, if the star is evolved, the isochrones and/or evolutionary tracks for the stellar models intersect themselves, resulting an ambiguous solution (i.e. it is not a “function” any more). For HAT-P-2, however, the solution of Eq. (15) is definite since the host star is a main sequence star. To obtain the physical parameters (e.g. the stellar radius), we used the stellar evolutionary models of Yi et al. (2001), by interpolating the values of  $\rho_*$ ,  $T_{\text{eff}}$  and [Fe/H] using the interpolator provided by Demarque et al. (2004).

The procedure described above has been applied to all of the parameters in the input set in a complete Monte-Carlo way (see also Pál et al. 2008a), where the values of  $\rho_0$  have been derived from the values of  $a/R_*$  and the orbital period  $P$  using Eq. (13), while the values for  $T_{\text{eff}}$  and [Fe/H] have been drawn from Gaussian random variables with the mean and standard deviation of the first SME results ( $T_{\text{eff}} = 6290 \pm 110$  K and [Fe/H] =  $0.12 \pm 0.08$ ). This step resulted the *a posteriori* distribution of the physical stellar parameters, including the surface gravity. The value and uncertainty for that was  $\log g_* = 4.16 \pm 0.04$  (CGS), which is slightly smaller than the value provided by the SME analysis. To reduce the uncertainties in  $T_{\text{eff}}$  and [Fe/H], we repeated the SME modeling by fixing the value of  $\log g_*$  to the above. This second SME run resulted  $T_{\text{eff}} = 6290 \pm 60$  K and [Fe/H] =  $0.14 \pm 0.08$ . Following, we updated the values for the limb darkening parameters ( $\gamma_1^{(z)} = 0.1419$ ,  $\gamma_2^{(z)} = 0.3634$ ,  $\gamma_1^{(b+y)} = 0.4734$ ,  $\gamma_2^{(b+y)} = 0.2928$ ,  $\gamma_1^{(I)} = 0.1752$ , and  $\gamma_2^{(I)} = 0.3707$ ), and repeated the simultaneous light curve and radial velocity fit. The results of this fit were then used to repeat the stellar evolution modeling, which yielded among other parameters  $\log g_* = 4.138 \pm 0.035$  (CGS). Since the value for  $\log g_*$  did not change significantly, we accepted these stellar parameter values as a final ones. The stellar parameters are summarized in Table 2 and the light curve and

radial velocity parameters are listed in the top two blocks of Table 3.

#### 4.5 Planetary parameters

In the previous two steps of the analysis, we determined the light curve, radial velocity and stellar parameters. In order to get the planetary parameters, we combined the two Monte-Carlo data sets which yields their *a posteriori* distribution in a consistent way. For example, the mass of the planet is calculated using

$$M_p = \frac{2\pi K \sqrt{1-e^2}}{P G \sin i} \left( \frac{a}{R_\star} \right)^2 R_\star^2, \quad (16)$$

where the values for the period  $P$ , RV semi-amplitude  $K$ , eccentricity  $e$ , inclination  $i$ , and normalized semi-major axis  $a/R_\star$  were taken from the results of the light curve and RV fit while the values for  $R_\star$  were taken from the respective points of the stellar parameter distribution. From the distribution of the planetary parameters, we obtained the mean values and uncertainties. We derived  $M_p = 9.09 \pm 0.24 M_{\text{Jup}}$  for the planetary mass,  $R_p = 1.157^{+0.073}_{-0.062} R_{\text{Jup}}$  for the radius while the correlation between these parameters were  $C(M_p, R_p) = 0.68$ . The planetary parameters are summarized in the lower block of Table 3. Comparing to the values reported by Bakos et al. (2007a), the mass of the planet does not change significantly (from  $M_p = 9.04 \pm 0.50 M_{\text{Jup}}$ ), but the respective uncertainty is smaller by a factor of two. The new estimation for the radius of the planet is larger by roughly  $2\text{-}\sigma$  while the uncertainty for the radius is slightly smaller (i.e.  $R_p = 0.982^{+0.038}_{-0.105} R_{\text{Jup}}$  for Bakos et al. 2007a).

Due to the eccentric orbit and the lack of the knowledge of the heat redistribution of the incoming stellar flux, the surface temperature of the planet can be constrained with difficulties. Assuming complete heat redistribution, the surface temperature can be estimated by time averaging the incoming flux which varies as  $1/r^2 = a^{-2}(1 - e \cos E)^{-2}$  due to the orbital eccentricity. The time average of  $1/r^2$  is

$$\left\langle \frac{1}{r^2} \right\rangle = \frac{1}{T} \int_0^T \frac{dt}{r^2(t)} = \frac{1}{2\pi} \int_0^{2\pi} \frac{dM}{r^2(M)}, \quad (17)$$

where  $M$  is the mean anomaly of the planet. Since  $r = a(1 - e \cos E)$  and  $dM = (1 - e \cos E)dE$ , where  $E$  is the eccentric anomaly, the above integral can be calculated analytically and the result is

$$\left\langle \frac{1}{r^2} \right\rangle = \frac{1}{a^2 \sqrt{1-e^2}}. \quad (18)$$

Using this time averaged weight for the incoming flux, we derived  $T_p = 1540 \pm 30$  K. However, the planet surface temperature would be  $\sim 2975$  K on the dayside during periastron and assuming no heat redistribution, while the equilibrium temperature would be only  $\sim 1190$  K if the planet was always at apastron. Thus, we conclude that the surface temperature can vary by a factor of  $\sim 3$ , depending on the actual atmospheric dynamics.

**Table 3.** Spectroscopic and light curve solutions for HAT-P-2, and inferred planetary parameters.

Parameter	Value
Light curve parameters	
$P$ (days)	$5.6334729 \pm 0.0000061$
$E$ (BJD - 2,400,000)	$54,387.49375 \pm 0.00074$
$T_{14}$ (days) <sup>a</sup>	$0.1787 \pm 0.0013$
$T_{12} = T_{34}$ (days) <sup>a</sup>	$0.0141^{+0.0015}_{-0.0012}$
$a/R_\star$	$8.99^{+0.39}_{-0.41}$
$R_p/R_\star$	$0.07227 \pm 0.00061$
$b \equiv (a/R_\star) \cos i (1 - e^2)/(1 + h)$	$0.395^{+0.080}_{-0.123}$
$i$ (deg)	$86^\circ.72^{+1.12}_{-0.87}$
Spectroscopic (RV) parameters	
$K$ (m s <sup>-1</sup> )	$983.9 \pm 17.2$
$k \equiv e \cos \omega$	$-0.5152 \pm 0.0036$
$h \equiv e \sin \omega$	$-0.0441 \pm 0.0084$
$e$	$0.5171 \pm 0.0033$
$\omega$	$185.22^\circ \pm 0.95^\circ$
Planetary parameters	
$M_p$ ( $M_{\text{Jup}}$ )	$9.09 \pm 0.24$
$R_p$ ( $R_{\text{Jup}}$ )	$1.157^{+0.073}_{-0.062}$
$C(M_p, R_p)$	0.68
$\rho_p$ (g cm <sup>-3</sup> )	$7.29 \pm 1.12$
$a$ (AU)	$0.06878 \pm 0.00068$
$\log g_p$ (cgs)	$4.226 \pm 0.043$
$T_{\text{eff}}$ (K)	$1540 \pm 30$ (see <sup>b</sup> )
Secondary eclipse	
$\phi_{\text{sec}}$	$0.1868 \pm 0.0019$
$E_{\text{sec}}$ (BJD - 2,400,000)	$54,388.546 \pm 0.011$
$T_{14,\text{sec}}$ (days)	$0.1650 \pm 0.0034$

<sup>a</sup>  $T_{14}$ : total transit duration, time between first to last contact;  $T_{12} = T_{34}$ : ingress/egress time, time between first and second, or third and fourth contact.

<sup>b</sup> This effective temperature assumes uniform heat redistribution while the irradiance is averaged on the orbital revolution. See text for further details about the issue of the planetary surface temperature.

#### 4.6 Photometric parameters and the distance of the system

The stellar evolution modeling (see § 4.4) also yields the absolute magnitudes and colors for the models for various photometric passbands. We compared the obtained colors and absolute magnitudes with other observations. First, the  $V - I$  color of the modeled star was compared with the observations. The TASS catalogue (Droege et al. 2006) has magnitudes for this star,  $V_{\text{TASS}} = 8.71 \pm 0.04$  and  $I_{\text{TASS}} = 8.16 \pm 0.05$ , i.e. the observed color of the star is  $(V - I)_{\text{TASS}} = 0.55 \pm 0.06$ . The stellar evolution modeling resulted a color of  $(V - I)_{\text{YY}} = 0.552 \pm 0.016$ , which is in perfect agreement with the observations. The absolute magnitude of the star in  $V$  band is  $M_V = 3.31 \pm 0.13$ , also given by the stellar evolution models. This therefore yields a distance modulus of  $V_{\text{TASS}} - M_V = 5.39 \pm 0.13$ , which is equivalent to a distance of  $119 \pm 8$  pc, assuming no interstellar reddening. This distance value for the star is placed right between the distance values found in the two different available Hipparcos reductions of Perryman et al. (1997) and van Leeuwen (2007a,b): Perryman et al. (1997) reports a parallax of  $7.39 \pm 0.88$  mas, equivalent to a dis-



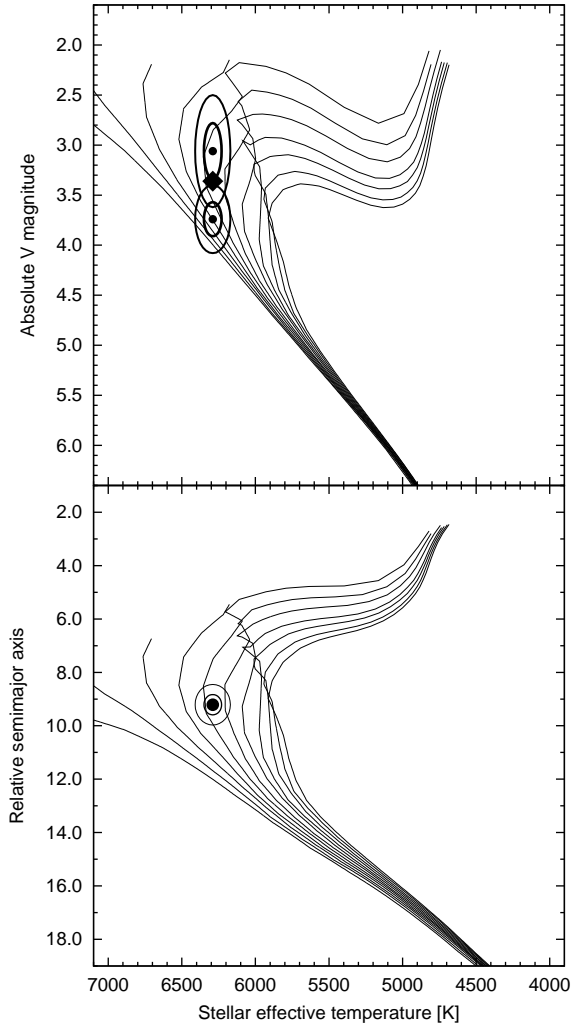


**Figure 5.** Stellar evolutionary isochrones from the Yonsei-Yale models, showing the isochrones for  $[\text{Fe}/\text{H}] = 0.14$  stars, between 0.5 and 5.5 Gyrs (with a cadence of 0.5 Gyrs). The color is indicated by the effective temperature, while the upper panel shows the luminosity using the absolute V magnitude  $M_V$  and the lower panel uses the ratio  $a/R_*$  as a luminosity indicator. In the upper panel, the isochrones are over-plotted by the 1- $\sigma$  and 2- $\sigma$  confidence ellipsoids, defined by the effective temperature, and the absolute magnitude estimations from the TASS catalogue and the two Hipparcos reductions (older: upper ellipse, recent: lower ellipse). The diamond indicates the  $M_V$  magnitude derived from our best fit stellar evolution models. On the lower plot, the confidence ellipsoid for the effective temperature and our estimation for  $a/R_*$  is shown.

tance of  $135 \pm 18$  pc while van Leeuwen (2007a,b) states a parallax of  $10.14 \pm 0.73$  mas, equivalent to a distance of  $99 \pm 7$  pc. In the two panels of Fig. 5, stellar evolutionary isochrones are shown for the metallicity of HAT-P-2, superimposed by the effective temperature and various luminosity estimations based on both the above discussion (relying only on various Hipparcos distances and TASS apparent magnitudes) and the constraints yielded by the stellar evolution

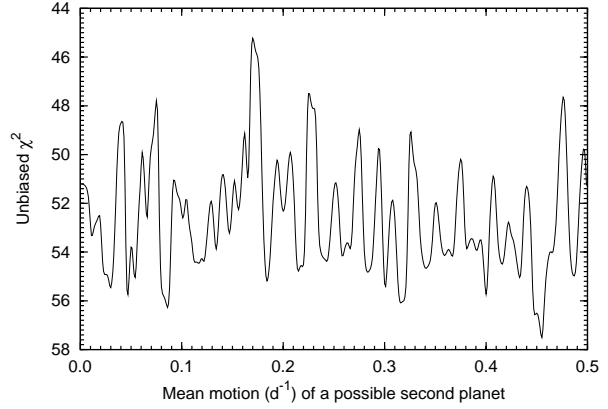


**Figure 6.** Unbiased residuals of a three-body Keplerian + circular fit to the RV observations where the mean motion of a possible secondary companion has been varied between 0 and  $0.5 \text{ d}^{-1}$ .

modelling. The 2MASS magnitude of the star in  $J$  band is  $J_{2\text{MASS}} = 7.822 \pm 0.027$  (converted to the ESO system, see Carpenter 2001), while the stellar evolution models yielded an absolute magnitude of  $M_J = 2.41 \pm 0.12$ . Thus, the distance modulus here is  $J_{2\text{MASS}} - M_J = 5.35 \pm 0.13$ , equivalent to a distance of  $120 \pm 8$  pc, confirming the distance derived from the photometry taken from the TASS catalogue.

#### 4.7 Signs for a second companion

As a final step of the analysis, we checked how can we constrain the presence of another, planetary companion around the star HAT-P-2. We performed two types of tests. In both of these tests we have fitted the RV semi-amplitude  $K$ , the Lagrangian orbital elements ( $k, h$ ), the three zero-point velocities ( $\gamma_{\text{Keck}}$ ,  $\gamma_{\text{Lick}}$  and  $\gamma_{\text{OHP}}$ ) and the additional terms required by the respective test methods (drift coefficients or orbital amplitudes). In these fits, the orbital epoch  $E$  and period  $P$  of HAT-P-2b have been kept fixed to the values yielded by the joint photometric and RV fit. This is a plausible assumption since without the constraints given by the photometry, the best fit epoch and period would be  $E_{\text{RV}} = 2454342.455 \pm 0.016$  (BJD) and  $P = 5.6337 \pm 0.0016$ , i.e. the uncertainties would be roughly 20 – 25 times larger.

In the first test, a linear, quadratic and cubic polynomial were added to the radial velocity model functions in addition to the  $\gamma$  zero-point velocities. Fitting a linear trend yielded a drift of  $G_{\text{linear}} = -21.2 \pm 12.1 \text{ m s}^{-1} \text{ yr}^{-1}$  while the unbiased  $\chi^2$  have been decreased from 52.1 to 48.5 (note that in this test the effective degrees of freedom is  $45 - 7 = 38$ ), so both the decrease in the residuals and the relative uncertainty of  $G_{\text{linear}}$  suggest a noticeable but not very significant existence of a slow linear drift on the timescale of the observations (that is, approximately, 1.7 years). The additional quadratic and cubic terms do not yield a significant decrease in the unbiased residuals.

In the second test, we extended the system configuration with an additional planet orbiting the star on a circular orbit. The orbital phase and the semi-amplitude of this additional companion was fitted simultaneously with the Keplerian orbital elements of HAT-P-2b while the mean mo-

tion of the second companion was varied between  $n_2 = 0$  and  $n_2 = 0.5 \text{ d}^{-1} \approx 0.45 n_{\text{HAT-P-2}}$  with a stepsize of  $\Delta n = 0.001 \text{ d}^{-1} < (1.7 \text{ yr})^{-1}$ . As it can be seen on Fig. 6, no significant detection of a possible secondary companion can be confirmed.

#### 4.8 Secondary eclipse timings

The improved orbital eccentricity and argument of pericenter allow us to estimate the time of the possible occultations. As it is known from the literature (see e.g. Charbonneau et al. 2005), for small orbital eccentricities, the offset of the secondary eclipse is proportional to  $k = e \cos \omega$ . However, in the case of larger eccentricities, like for HAT-P-2b, this linear approximation cannot be applied. The appropriate formula for arbitrary eccentricities can be calculated as a difference between the mean orbital longitudes at secondary eclipses ( $\lambda_{\text{sec}}$ ) and transits ( $\lambda_{\text{pri}}$ ), that is

$$\lambda_{\text{sec}} - \lambda_{\text{pri}} = \pi + \frac{2kJ}{1-h^2} + \arg \left[ J^2 + \frac{k^2 e^2}{(1+J)^2} - \frac{2k^2}{1+J}, 2k - \frac{2e^2 k}{1+J} \right], \quad (19)$$

where  $J = \sqrt{1-e^2}$ . It is easy to see that the expansion of Eq. (19) yields

$$\lambda_{\text{sec}} - \lambda_{\text{pri}} \approx \pi + 4k \quad (20)$$

for  $|k| \ll 1$  and  $|h| \ll 1$  and this is equivalent with Eq. (3) of Charbonneau et al. (2005). In the case of HAT-P-2b, we found that secondary eclipses occur at the orbital phase of  $\phi_{\text{sec}} = (\lambda_{\text{sec}} - \lambda_{\text{pri}})/(2\pi) = 0.1868 \pm 0.0019$ , i.e. 1 day 1 hour and 17 minutes ( $\pm 15$  minutes) after primary transit events.

## 5 DISCUSSION

We presented refined planetary, stellar and orbital parameters for the HAT-P-2(b) transiting extrasolar planetary system. Our improved analysis was based on numerous radial velocity data points, including both new measurements and data taken from the literature, plus a new data-set of high precision photometry follow-up observations. The refined parameters have uncertainties smaller by a factor of  $\sim 2$  in the planetary parameters and a factor of  $\sim 3-4$  in the orbital parameters than the previously reported values of Bakos et al. (2007a). We note that the density of the planet turned out to be significantly smaller than the value by Bakos et al. (2007a), namely  $\rho_p = 7.6 \pm 1.1 \text{ g cm}^{-3}$ , moreover, the uncertainty reported by Bakos et al. (2007a) was significantly larger (that value for the density of the planet was  $\rho_{p,B2007} = 11.9^{+4.8}_{-1.6} \text{ g cm}^{-3}$ ). In our analysis we did not rely on the distance of the system, i.e. we did not use the absolute magnitude as a luminosity indicator. Instead, our stellar evolution modeling was based on the density of the star, an other luminosity indicator related to precisely observable light curve and RV parameters. We have compared the estimated distance of the system (which was derived from the absolute magnitudes, known from the stellar modeling) with the Hipparcos distances. We found that our newly estimated distance falls between the two values available from the different reductions of Hipparcos raw data.

The zero insolation planetary isochrones of

Baraffe et al. (2003) give an expected radius of  $R_{p,\text{Baraffe03}} = 1.02 \pm 0.02 R_{\text{Jup}}$ , which is slightly smaller than the measured radius of  $1.16^{+0.07}_{-0.06} R_{\text{Jup}}$ . The work of Fortney, Marley & Barnes (2007) takes into account not only the evolutionary age and the total mass of the planet but the incident stellar flux and the mass of the planet's core. By scaling the semi-major axis of HAT-P-2b to one that yields the same incident flux from a solar-type star on a circular orbit, taking into account both the luminosity of the star and the correction for the orbital eccentricity given by Eq. (18), we derived  $a' = 0.033 \pm 0.003 \text{ AU}$ . Using this scaled semimajor axis, the interpolation based on the tables provided by Fortney, Marley & Barnes (2007) yields radii between  $R_{p,\text{Fortney,0}} = 1.142 \pm 0.003 R_{\text{Jup}}$  (core-less planets) and  $R_{p,\text{Fortney,100}} = 1.111 \pm 0.003 R_{\text{Jup}}$  (core-dominated planets, with a core of  $M_{p,\text{core}} = 100 M_{\oplus}$ ). Although these values agree nicely with our value of  $R_p = 1.157^{+0.073}_{-0.062} R_{\text{Jup}}$ , the relatively large uncertainty of  $R_p$  excludes any further conclusion for the size of the planet's core. Recent models of Baraffe, Chabrier & Barman (2008) also give the radius of the planet as the function of evolutionary age, metal enrichment and an optional insolation for equivalent to scaled semi-major axis of  $a' = 0.045 \text{ AU}$ . Using this latter insolation, their models yield  $R_{p,\text{Baraffe08,0.02}} = 1.055 \pm 0.006 R_{\text{Jup}}$  (for metal poor,  $Z = 0.02$  planets) and  $R_{p,\text{Baraffe08,0.10}} = 1.008 \pm 0.006 R_{\text{Jup}}$  (for more metal rich,  $Z = 0.10$  planets). These values are slightly smaller than the actual radius of HAT-P-2b, however, the actual insolation of HAT-P-2b is roughly two times larger than the insolation implied by  $a' = 0.045 \text{ AU}$ . Since the respective planetary radii of Baraffe, Chabrier & Barman (2008) for zero insolation gives  $R_{p,\text{Baraffe08,0.02}}^{(0)} = 1.009 \pm 0.006 R_{\text{Jup}}$  and  $R_{p,\text{Baraffe08,0.10}}^{(0)} = 0.975 \pm 0.006 R_{\text{Jup}}$  for the respective cases of  $Z = 0.02$  and  $Z = 0.10$  metal enrichment, an extrapolation for a two times larger insolation would put the expected planetary radius in the range of  $\sim 1.10 R_{\text{Jup}}$ . This is consistent with the models of Fortney, Marley & Barnes (2007) as well as with the measurements. However, as discussed earlier in the case of the Fortney, Marley & Barnes (2007) models, the uncertainty in  $R_p$  does not allow us to properly constrain the metal enrichment for the recent Baraffe models.

HAT-P-2b will remain an interesting target, as a member of an emerging heavy-mass population. Further photometric measurements will refine the light curve parameters and therefore more precise stellar parameters can also be obtained. This will yield smaller uncertainties in the physical planetary radius, thus some parameters of the planetary evolution models, such as the metal enrichment can be obtained more explicitly. Moreover, observations of secondary eclipses will reveal the planetary atmosphere temperature which now is poorly constrained. Since the secondary eclipse occurs shortly after periastron passage, the temperature and therefore the contrast might be high enough to detect the occultation with a good signal-to-noise ratio. Moreover, as careful analysis of the RV data series has suggested a possible long-term drift, collecting further data points may confirm the presence of an additional, long-period companion orbiting the host star.

## ACKNOWLEDGMENTS

The work by A.P. was supported by the HATNet project and in part by ESA grant PECS 98073. HATNet operations have been funded by NASA grants NNG04GN74G, NNX08AF23G and SAO IR&D grants. Work of G.Á.B. and J. Johnson were supported by the Postdoctoral Fellowship of the NSF Astronomy and Astrophysics Program (AST-0702843 and AST-0702821, respectively). We acknowledge partial support also from the Kepler Mission under NASA Cooperative Agreement NCC2-1390 (D.W.L., PI). We thank Matt Holman and Josh Winn for swapping FLWO 1.2m telescope time. This research has made use of Keck telescope time granted through NOAO and NASA. We thank the UCO/Lick technical staff for supporting the remote-observing capability of the Nickel Telescope, allowing the photometry to be carried out from UC Berkeley. Automated Astronomy at Tennessee State University has been supported long-term by NASA and NSF as well as Tennessee State University and the State of Tennessee through its Centers of Excellence program. We acknowledge the use of the Vizier service (Ochsenbein et al. 2000) operated at CDS, Strasbourg, France, of NASA's Astrophysics Data System Abstract Service, and of the 2MASS Catalog.

## REFERENCES

- Bakos, G. Á., Lázár, J., Papp, I., Sári, P., & Green, E. M. 2002, *PASP*, 114, 974
- Bakos, G. Á., Noyes, R. W., Kovács, G., Stanek, K. Z., Sasselov, D. D., & Domsa, I. 2004, *PASP*, 116, 266
- Bakos, G. Á. et al. 2007, *ApJ*, 670, 826
- Bakos, G. Á. et al. 2007, *ApJ*, 671, L173
- Bakos, G. Á. et al. 2009, *ApJ*, submitted (arXiv:0901.0282)
- Baraffe, I. et al. 2003, *A&A*, 402, 701
- Baraffe, I., Chabrier, G. and Barman, T. 2008, *A&A*, 482, 315
- Barnes, J. W., 2007, *PASP*, 119, 986
- Barbieri, M. et al. 2007, *A&A*, 476, L13
- Borucki, W. J. et al., 2007, *ASP Conf. Ser.*, 366, 309
- Butler, R. P., Marcy, G. W., Williams, E. et al. 1996, *PASP*, 108, 500
- Carpenter, J. 2001, *AJ*, 121, 2851
- Charbonneau, D. et al. 2005, *ApJ*, 626, 523
- Claret, A. 2000, *A&A*, 363, 1081
- Claret, A. 2004, *A&A*, 428, 1001
- D'Angelo, G., Lubow, S. H. & Bate, M. R., 2006, *ApJ*, 652, 1698
- Demarque et al. 2004, *ApJS*, 155, 667
- Droege, T. F., Richmond, M. W., & Sallman, M. 2006, *PASP*, 118, 1666
- Fabrycky, D. & Tremaine, S. 2007, *ApJ*, 669, 1298
- Ford, E. B. & Rasio, F. A. 2008, *ApJ*, 686, 621
- Fortney, J. J., Marley, M. S. & Barnes, W. 2007, *ApJ*, 659, 1661
- Gillon, M. et al. 2007, *A&A*, 472, L13
- Hébrard, G., et al. 2008, *A&A*, 488, 763
- Henry, G. W. 1999, *PASP*, 111, 845
- Johns-Krull, C. M. et al. 2008, *ApJ*, 677, 657
- Johnson, J. A. et al. 2008, *ApJ*, 686, 649
- Kopal, Z. 1959, *Close Binary Systems* (New York: Wiley), p. 383
- Loeb, A., 2005, *ApJ*, 623, L45
- Loeillet, B. et al., 2008, *A&A*, 481, 529
- Mandel, K., & Agol, E. 2002, *ApJ*, 580, L171
- Naef, D. et al. 2001, *A&A*, 375, 27
- Ochsenbein, F., Bauer, P., & Marcout, J. 2000, *A&AS*, 143, 23
- Pál, A., & Bakos, G. Á. 2006, *PASP*, 118, 1474
- Pál, A., Süli, Á., 2007, *MNRAS*, 381, 1515
- Pál, A. et al., 2008, *ApJ*, 680, 1450
- Pál, A., Bakos, G. Á., Noyes, R. W. & Torres, G. 2008, *Proceedings of the IAU 253 Symposium "Transiting planets"*, ed. by F. Pont, *IAUS* 253, 428
- Pál, A. 2008, *MNRAS*, 390, 281
- Pál, A. 2009, *MNRAS*, 396, 1737
- Pál, A. PhD thesis (arXiv:0906.3486)
- Perryman, M. A. C., et al., 1997, *A&A*, 323, 49
- Press, W. H., Teukolsky, S. A., Vetterling, W. T. & Flannery, B. P., 1992, *Numerical Recipes in C: the art of scientific computing*, Second Edition, Cambridge University Press
- Sozzetti, A., Torres, G., Charbonneau, D., Latham, D. W., Holman, M. J., Winn, J. N., Laird, J. B., & O'Donovan, F. T. 2007, *ApJ*, 664, 1190
- Skrutskie, M. F. et al., 2006, *AJ*, 131, 1163
- Shporer, A., Mazeh, T., Moran, A., Bakos, G. Á., Kovács, G. & Mashal, E., 2006, Tenth Anniversary of 51 Peg-b: Status of and prospects for hot Jupiter studies, eds. L. Arnold, F. Bouchy and C. Moutou (Frontier Group, Paris), 196
- Takeda, G., Kita, R. & Rasio, F. A. 2008, *ApJ*, 683, 1063
- Valenti, J. A., & Fischer, D. A. 2005, *ApJS*, 159, 141
- Valenti, J. A., & Piskunov, N. 1996, *A&AS*, 118, 595
- van Leeuwen, F., 2007, *Hipparcos, the New Reduction of the Raw Data*, *Astrophysics and Space Science Library*, Vol. 250
- van Leeuwen, F., 2007, *A&A*, 474, 653
- Vogt, S. S., 1987, *PASP*, 99, 1214
- Vogt, S. S. et al. 1994, *Proc. SPIE*, 2198, 362
- Winn, J. N. et al. 2007, *ApJ*, 665, 167
- Winn, J. N. et al. 2007, *AJ*, 134, 1707
- Winn, J. N. et al. 2009a, *ApJ*, 700, 302
- Winn, J. N. et al. 2009b, *ApJ*, submitted (arXiv:0907.5205)
- Yi, S. K., Demarque, P., Kim, Y.-C., Lee, Y.-W., Ree, C. H., Lejeune, T., & Barnes, S. 2001, *ApJS*, 136, 417